

High quality ion-induced secondary electron imaging for MeV nuclear microprobe applications

E. J. Teo,^{a)} M. B. H. Breese, A. A. Bettiol, and F. Watt

Centre for Ion Beam Applications, Department of Physics, National University of Singapore, Singapore 117542

L. C. Alves

ITN Departamento de Fisica, E.N. 10, 2686-953 Sacavem, Portugal

(Received 10 June 2003; accepted 5 January 2004; published 25 February 2004)

The image quality of ion-induced secondary electron images generated with a MeV nuclear microprobe has previously been severely limited by the large beam current fluctuations produced by Van de Graaff accelerators. In this article we report the use of a solid state Cockroft–Walton type accelerator (HVEE™ Singletron) to produce high quality secondary electron images in a rapid manner. This has been achieved using a voltage-modulated dc signal imaging process rather than the inefficient pulse counting mode commonly used in nuclear microprobe applications. This is made possible because of the superior voltage stability of the Singletron accelerator resulting in higher ion beam current stability. Excellent topographical contrast has been demonstrated with the newly implemented secondary electron system. © 2004 American Vacuum Society.

[DOI: 10.1116/1.1651549]

I. INTRODUCTION

Imaging of secondary electrons induced by a focused MeV ion beam is able to provide topographical information, which is important for the identification of regions of interest and interpretation of spatially resolved images collected using high energy ion beam techniques such as particle-induced x-ray emission (PIXE) or Rutherford backscattering spectrometry (RBS). It also provides a rapid method of focusing the incident ion beam owing to the large electron flux emitted from surface features of, for example, calibration standards. In view of the valuable supplementary information that topographical imaging gives to high energy ion beam techniques, there has been considerable effort by many groups in developing ion-induced secondary electron imaging systems for use with a nuclear microprobe. Images can be generated either in a “pulse-counting” mode, whereby the image contrast depends on small number of secondary electron pulses recorded at each scan position, or a “voltage-modulated” dc mode whereby the image contrast is controlled by variations in a large, continuous secondary electron flux as the beam scans across the sample.

As voltage-modulated images are generated pixel by pixel in a sequential manner, this approach is adversely sensitive to beam current fluctuations on a millisecond scale. Typically, the ion beam produced from a Van de Graaff accelerator has large current fluctuations of $\pm 30\%$ about the mean value, at frequencies of several hundred Hz.^{1,2} This severely limits the contrast of the secondary electron images. Hence it is important to control the ion beam current fluctuations, or at least correct for them.^{1,3}

There has been considerable success with imaging of ion-induced secondary electrons in the pulse-counting mode, since the signal output can be easily integrated into existing

nuclear electronics and does not require a separate data acquisition system. In this approach, the image is acquired randomly over long data collection periods of many seconds. Variations in signal intensity due to beam current fluctuations tend to average out with time, so the images become less sensitive to beam fluctuations and reasonable topographical contrast has been obtained using this method.^{4–7} However, the number of electrons that contribute to the image is fundamentally limited by the data acquisition counting rate and dead time, resulting in statistically noisier images when compared to voltage-modulated images.

The aim of this work is to obtain high signal-to-noise ratio, ion-induced electron images using the Single-ended (Singletron™) accelerator at the National University of Singapore. Voltage multiplication is based on the Cockroft–Walton principle and does not rely on any mechanical moving parts. This accelerator has inherently low voltage fluctuations and consequently small beam current fluctuations, making it ideally suited to secondary electron imaging using a voltage-modulated mode. With the recently attained lateral beam resolution of 100 nm with our microprobe coupled to the Singletron accelerator,⁸ it is now possible to produce secondary electron images with high topographical contrast and spatial resolution.

Investigations are carried out on a patterned SiGe sample to determine the optimum signal-to-noise ratio that can be achieved by minimizing the beam fluctuations and increasing the signal intensity. For comparison, secondary electron images of a Cu grid are collected in both voltage-modulated and pulse-counting modes to demonstrate the improved image quality of the newly developed system. In the last section of this article, this new system is combined with ionoluminescence imaging to correlate the crystal faces and luminescence properties of chemical vapor deposition (CVD) synthetic diamond.

^{a)}Electronic mail: phytej@nus.edu.sg

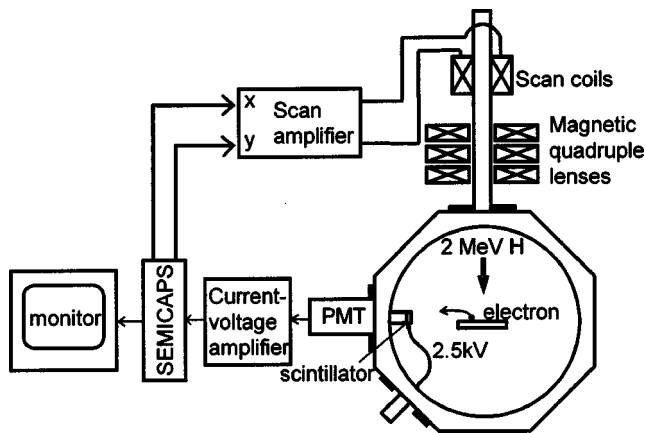


FIG. 1. Schematic diagram of the ion-induced secondary electron detection and image collection system used in the NUS microprobe facility.

II. EXPERIMENTAL PROCEDURES

Secondary electrons created during 2 MeV proton bombardment are detected by a H3165-10 Hamamatsu photomultiplier tube (PMT) via a P47 scintillator screen placed in front of the PMT (see Fig. 1). The current output of the PMT is amplified by a sensitive Hamamatsu C2719 current-to-voltage amplifier before being fed into a scanning electron microscopy image collection and processing system (SEMICAPS).⁹ The image is displayed with a pixel resolution of 512×512 , whereby the brightness is modulated by the amplified dc signal voltage level from the PMT. Point averaging is performed over a 512 sampling rate, which corresponds to a time of $130 \mu\text{s}$ per pixel. In this way, small random intensity fluctuations in the image can be averaged out.

III. RESULTS

By minimizing the beam current fluctuations produced by the Singletron accelerator, it is possible to reduce the noise in the signal output and hence improve the signal-to-noise ratio of the electron image. The most important accelerator parameter which affects the beam current fluctuations of our Singletron was found to be the ion source gas pressure. The beam current was measured from a Faraday cup located after the 90° bending magnet, which was then converted into a dc signal with a current-to-voltage amplifier before display on an oscilloscope. By monitoring the change of the voltage level with time, it is possible to determine the amplitude and frequency of the beam fluctuations. Figures 2(a) and 2(b) show the oscilloscope traces for the beam current at source gas pressures of 9.1×10^{-7} and 1.5×10^{-6} mBar, respectively. While the average beam intensity stays about the same for both gas pressures, it can be seen that the 400 and 50 Hz periodic noise observed at 9.1×10^{-7} mBar is significantly reduced after increasing the gas pressure to 1.5×10^{-6} mBar. The 400 Hz noise originates from the motor generator system that is used to power the ion source and the 50 Hz noise arises from the mains power supply. Similar noise patterns have been observed by the same accelerator

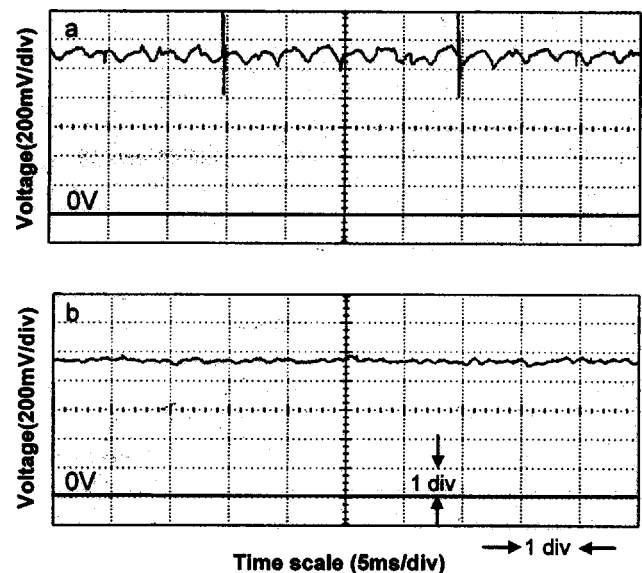


FIG. 2. Oscilloscope traces of the signal intensity at gas pressures of (a) 9.1×10^{-7} mBar and (b) 1.5×10^{-6} mBar.

used in Leipzig.¹⁰ At a gas pressure of 9.1×10^{-7} mBar, the 400 Hz noise introduces a $\pm 5\%$ fluctuation in the beam intensity over a periodic interval of 2 ms. Since the dwell time of the beam for each pixel is about $100 \mu\text{s}$, this means that the signal intensities will oscillate sinusoidally every 20 pixels. These periodic changes in signals are sufficient enough to mask small variations in the ion-induced electron signal due to topographical contrast. By increasing the gas pressure while keeping other accelerator parameters constant, the 400 Hz periodic noise was significantly reduced to $\pm 2\%$. This represents the minimum level of fluctuation which we have achieved with the Single-ended accelerator, being more than ten times better than that obtained from Van de Graaff accelerators. A conventional belt-driven Van de Graaff accelerator typically suffers from 1 to 5 kV instability in terminal voltage¹¹ due to the unevenness of the charging system, which increases with age. This results in large beam fluctuations of $\pm 25\% - 34\%$.^{1,2} With the superior voltage stability of 20 V produced with a solid-state Cockroft-Walton type accelerator,¹⁰ it is possible to obtain more stable beam intensity.

The effect of the beam fluctuations can be seen in the ion-induced electron images of a patterned SiGe sample in Fig. 3, which were collected using the two gas pressures discussed in Fig. 2. Alternating dark bands appear in Fig. 3(a), and this striped effect is significantly reduced at higher gas pressure in Fig. 3(b), resulting in a much smoother image. Line scans extracted from the flat regions of the sample showed that the signal-to-noise signal improved from 6:1 to 10:1 when the beam fluctuations were reduced from $\pm 5\%$ to $\pm 2\%$.

The signal-to-noise ratio can also be increased using a larger analyzing beam current. Figures 4(a) and 4(b) show the line profiles measured across a flat region of the SiGe electron images collected at beam currents of 20 and 100 pA, respectively. The intensity of the beam current was varied by

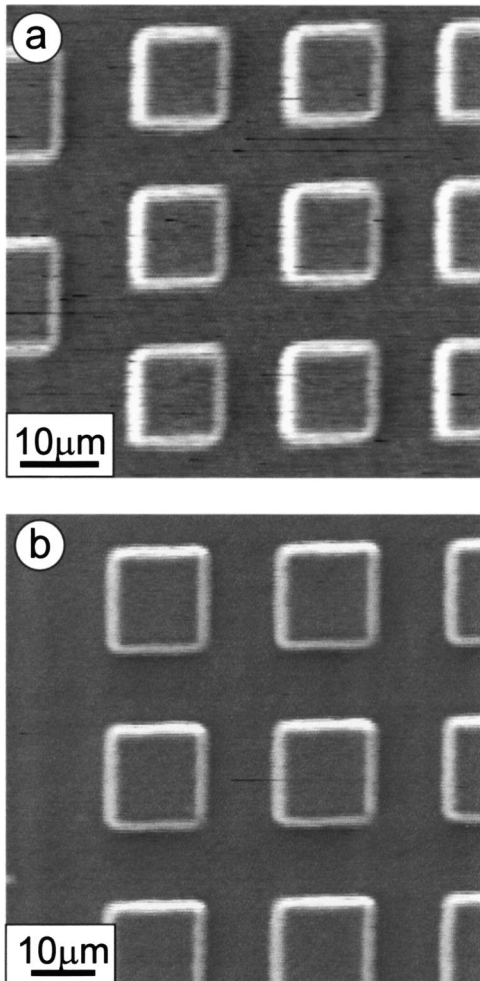


FIG. 3. Ion-induced secondary electron images of a patterned SiGe mesa sample collected with a beam fluctuation of (a) $\pm 5\%$ and (b) $\pm 2\%$.

changing the size of the microprobe collimator slits, so as to keep all the accelerator parameters constant. It can be seen that fluctuations reduce from 23% to 12% as the beam current intensity is increased from 20 to 100 pA. Signal-to-noise ratio is improved due to the higher signal voltage level and reduction of dark current from a lower PMT gain used. Based on these images, we have found that an ion beam current of more than 20 pA helps to produce high quality images. Incidentally, beam currents in excess of 100 pA are typically used to perform micro PIXE and RBS, making it compatible with this technique. Assuming the detection system has a bandwidth of about 7.7 kHz, the shot noise is found to be less than 1% for an incident beam current of 20 pA. This constitutes a small effect to the overall noise fluctuation and can thus be ignored.

Secondary electron imaging was performed on a 2000 mesh Cu calibration grid in both voltage-modulated and pulse-counting mode to compare the image quality using the two different approaches. In pulse-counting mode, the secondary electrons were detected as transistor-transistor logic pulses with a channel electron multiplier and connected directly into the microprobe data acquisition system.¹² Reference 13 gives a detailed description of this detection system.

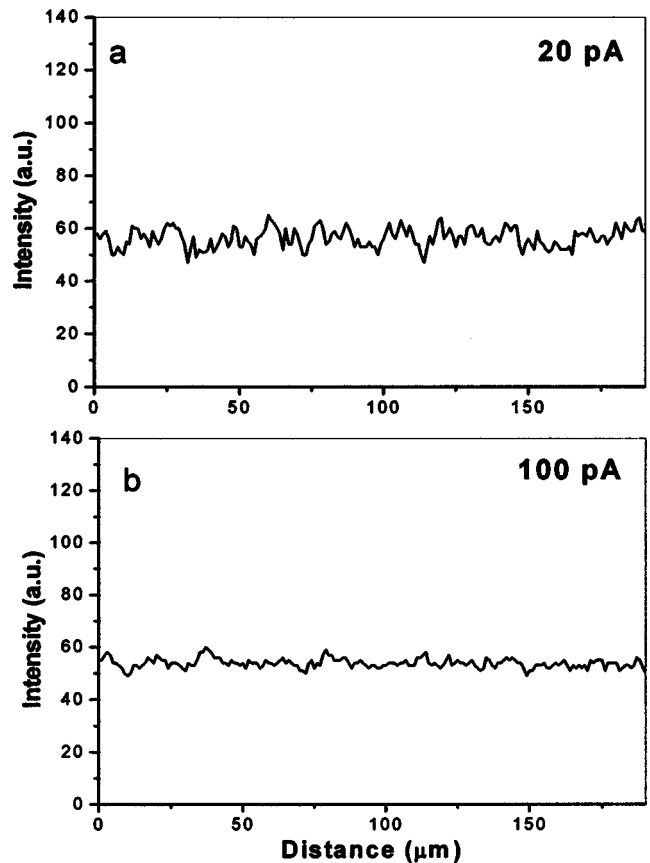


FIG. 4. Line profiles measured across a flat region in the SiGe electron image, which is collected at a beam current of (a) 20 pA and (b) 100 pA.

It can be seen that Fig. 5(a) appears statistically noisier compared with Fig. 5(b). Some topography information is lost in pulse-counting mode as the resultant number of electrons contributing to the image is small, limited by the data acquisition counting rate of several kHz. No such limitation applies in voltage-modulated mode, and the much greater number of secondary electrons, which contribute to the image, result in much smoother images. In general, electrons can be detected with an electron multiplier or PMT. However, the electron multiplier tends to saturate at a lower current and is more suitable for imaging in very low current mode (< 1 pA).

Another advantage of the greatly increased counting statistics obtained in voltage-modulated mode compared with pulse-counting mode is the shorter collection time required for each image. It takes about 3 s to obtain the electron image of the grid in dc mode as compared to 30 s in the pulse counting mode. This means that real time focusing of the ion beam can be achieved with the new imaging system, making it an indispensable technique for rapid optimization of the beam before analysis by other nuclear microprobe techniques. For samples that are susceptible to beam damage, this provides a quick way for locating regions of interests.

The new ion-induced secondary electron imaging system was combined with an ionoluminescence imaging system¹³ to correlate the luminescence properties and crystal faces of

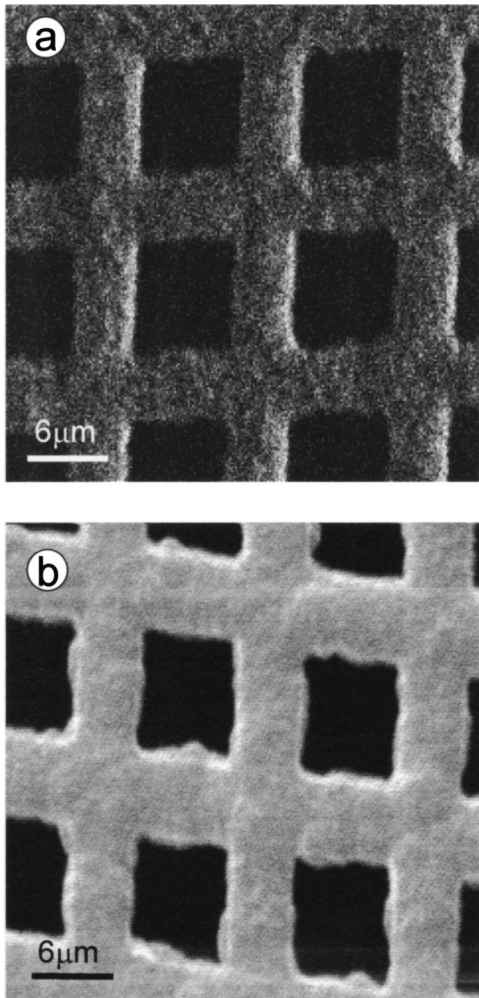


FIG. 5. Comparison of the electron image of a copper grid (with periodicity of $12.7 \mu\text{m}$) collected in (a) pulse-counting mode and (b) voltage-modulated mode.

a CVD grown diamond film. A large-area ion-induced secondary-electron image of the diamond film in Fig. 6(a) shows that the sample consists of many crystallites averaging about $40 \mu\text{m}$ in dimension. Figures 6(b) and 6(c), respectively, show secondary electron and luminescence imaging at 575 nm of a single diamond crystallite. It is observed that orange luminescence tends to be associated with the square (100) faces of the crystallite. The triangular (111) faces emit less strongly at 575 nm wavelength. This luminescence peak is the zero phonon line of a well-known system often observed in CVD diamond¹⁴ and has been attributed to the nitrogen-vacancy complex.¹⁵ Our results are consistent with other groups who found a strong correlation between the 575 nm emission and the single crystal (100) growth faces.^{14,16,17} Less emission has been seen from (111) faces which tend to contain more dislocations and faults.

IV. CONCLUSIONS

A new secondary electron imaging system based on voltage-modulated signal output has been developed for focused high energy MeV ion beam applications. High signal-

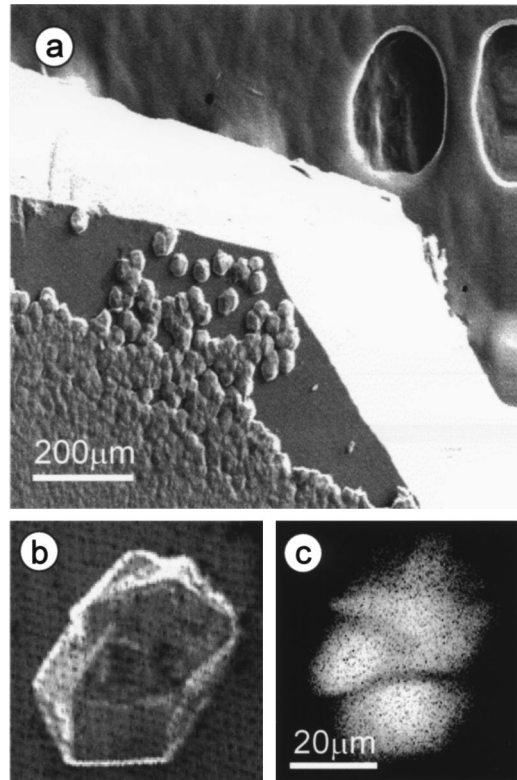


FIG. 6. (a) $1 \times 1 \text{ mm}$ image of a synthetic diamond grown by chemical vapor deposition. (b) Ion-induced secondary electron image and (c) ionoluminescence image at wavelength 575 nm of a single diamond crystallite.

to-noise ratio secondary electron images have been obtained by reducing accelerator beam current fluctuations to $\pm 2\%$ and using beam currents of more than 20 pA . This is a better imaging mode than the more commonly used pulse counting mode because of the better topographical contrast due to the higher counting statistics and shorter collection time. Real time focusing of the ion beam can be achieved with the newly implemented system. The use of ion-induced electron imaging with other nuclear techniques also helps in the interpretation and understanding of the data obtained.

ACKNOWLEDGMENT

E. J. Teo would like to acknowledge the financial support by the Singapore Millennium Foundation.

- ¹P. A. Younger and J. A. Cookson, *Nucl. Instrum. Methods* **158**, 193 (1979).
- ²L. C. Alves, M. B. H. Breese, M. F. da Silva, and J. C. Soares, *Nucl. Instrum. Methods Phys. Res. B* **188**, 146 (2002).
- ³M. Takai, Y. Agawa, K. Ishibashi, K. Hirai, S. Namba, K. Inoue, and Y. Kawata, *Nucl. Instrum. Methods Phys. Res. B* **54**, 279 (1991).
- ⁴G. W. Grime, M. Dawson, M. Marsh, I. C. McArthur, and F. Watt, *Nucl. Instrum. Methods Phys. Res. B* **54**, 52 (1991).
- ⁵H. Kneis, B. Martin, R. Nobiling, B. Povh, and K. Traxel, *Nucl. Instrum. Methods Phys. Res.* **197**, 79 (1982).
- ⁶M. B. H. Breese, J. A. Cookson, J. A. Coyle, and A. E. Ledbury, *Nucl. Instrum. Methods Phys. Res. B* **54**, 12 (1991).
- ⁷E. J. Teo, M. Alkai, A. A. Bettiol, T. Osipowicz, J. Van. Kan, F. Watt, and A. Markwitz, *Nucl. Instrum. Methods Phys. Res. B* **190**, 339 (2002).
- ⁸F. Watt, J. A. van Kan, I. Rajta, A. A. Bettiol, T. F. Choo, M. B. H. Breese, and T. Osipowicz, *Nucl. Instrum. Methods Phys. Res. B* **210**, 14 (2003).

- ⁹J. C. H. Phang, K. K. W. Ong, D. S. H. Chan, T. S. Low, and N. F. Ng, *Proceedings of the International Symposium on the Physical and Failure Analysis of Integrated Circuits*, edited by D. Chan, K. P. Lim, and T. S. Low (IEEE Singapore, Singapore, 1987), pp. 50–61.
- ¹⁰D. J. W. Mous, R. G. Haitzma, T. Butz, R.-H. Flaymeyer, D. Lehmann, and J. Vogt, *Nucl. Instrum. Methods Phys. Res. B* **130**, 31 (1997).
- ¹¹F. Watt, I. Orlic, K. K. Loh, C. H. Sow, P. Thong, S. C. Liew, T. Osipowicz, T. F. Choo, and S. M. Tang, *Nucl. Instrum. Methods Phys. Res. B* **85**, 708 (1994).
- ¹²G. W. Grime and M. Dawson, *Nucl. Instrum. Methods Phys. Res. B* **89**, 223 (1994).
- ¹³E. J. Teo, A. A. Bettiol, C. N. B. Udalagama, and F. Watt, *Nucl. Instrum. Methods Phys. Res. B* **210**, 501 (2003).
- ¹⁴V. S. Vavilov, A. A. Gippius, A. M. Zaitsev, B. V. Deryagin, B. V. Spitsyn, and A. E. Aleksenko, *Sov. Phys. Semicond.* **14**, 1078 (1990).
- ¹⁵L. H. Robbins, L. P. Cook, E. N. Farabaugh, and A. Feldman, *Phys. Rev. B* **39**, 13367 (1989).
- ¹⁶H. Kanda, K. Watanabe, S. Koizumi, and T. Teraji, *Diamond Relat. Mater.* **12**, 20 (2003).
- ¹⁷R. J. Graham and K. V. Ravi, *Appl. Phys. Lett.* **60**, 1310 (1992).